

An X-ray and Radio Study of the Cluster A2717

H. Liang¹, M. Pierre¹, A. Unewisse^{2,3}, and R.W. Hunstead²

¹ CEA/DSM/DAPNIA CE Saclay, Service d'Astrophysique, F-91191 Gif sur Yvette, France

² School of Physics, The University of Sydney, NSW 2006, Australia

³ Electronic and Surveillance Research Lab., DSTO, Salisbury, SA 5108, Australia

Received ...

Abstract. We present an X-ray, radio and optical study of the cluster A2717. The central D galaxy is associated with a Wide-Angled-Tailed (WAT) radio source. A *Rosat* PSPC observation of the cluster shows that the cluster has a well constrained temperature of $1.9_{-0.2}^{+0.3} \times 10^7$ K. The pressure of the intracluster medium was found to be comparable to the minimum pressure of the radio source suggesting that the tails may in fact be in equipartition with the surrounding hot gas.

Key words: galaxies: clustering – clusters of galaxies: individual Abell 2717 – cosmology: observations – dark matter – radio galaxies– X-rays: galaxies

known properties of the cluster and its central D galaxy are summarised in Table 1 and 2.

Table 1. Optical data for the cluster A2717

Centre (J2000) ¹	RA = 00 03 12.4 Dec = -35 57 48
Bautz-Morgan class ²	I-II
Richness class ²	1
Redshift ³ , z_{cl}	0.0492 ± 0.0003
Velocity dispersion ³ , σ_{los}	547_{-72}^{+92} km s ⁻¹
Schechter characteristic mag ⁴ , M^*	-19.55 ± 0.25

¹ Centroid derived from COSMOS catalogue; ² Abell et al. 1989; ³ Colless & Hewett 1987; ⁴ Colless 1989.

1. Introduction

The intracluster media of clusters of galaxies can be probed directly by their X-ray emission and at the same time indirectly through the morphologies of the radio sources associated with cluster members. The physical nature of radio galaxies is reflected in the structure of their emission. Studies of radio galaxies have led to a better understanding of both radio emission processes and galaxy environments. One class of interesting radio sources is the Wide-Angle-Tailed (WAT) sources. Originally defined by Owen & Rudnick (1976), WATs are characterised by a radio structure composed of twin jets separated by a wide opening angle and are associated with the dominant member of a cluster of galaxies. They are radio sources with intermediate radio luminosities in the range 10^{42} to 10^{43} erg s⁻¹ (O'Donoghue 1990), comparable to the Fanaroff-Riley (1974) break between the FR class I and II. WATs are ideally suited for the study of galaxy/environment interactions. They are known to favour X-ray poor environments and almost never found in regions with cooling flows (Norman *et al.* 1988; Burns 1990; Zhao *et al.* 1990) despite being associated with galaxies most likely to be found in cooling flow regions. This implies that the radio emission and cluster gas are associated in some way.

The southern galaxy cluster A2717 has a central D galaxy which is associated with a WAT source. A2717 has been studied extensively in the optical (eg. Colless *et al.* 1987, 1989). The

Table 2. Optical data for the D galaxy of A2717

Position (J2000) ¹	RA = 00 03 12.7 Dec = -35 56 13
Redshift ² , z_{gal}	0.0497 ± 0.0001
Stellar dispersion ² , σ_s	258 ± 42 km s ⁻¹
Semi-major axis ³	36.1''
Semi-minor axis ³	34.4''
Position angle ³	136°
B_J magnitude ³	14.7

¹ Position measured from an AAT CCD image by R. Hunstead; ² Colless & Hewett 1987. ³ Results from COSMOS.

We present here radio and X-ray observations of the cluster. In the radio, it was originally imaged with the Molonglo Observatory Synthesis Telescope (MOST) at 843 MHz in September 1988 and the host galaxy of the WAT was found to be the dominant galaxy of the cluster. In June and October of 1989 two more images were made with the VLA in scaled arrays at 20 cm in C/D and 6 cm B/C in order to resolve the radio structure. Then, in 1992, a higher resolution image was obtained with the Australia Telescope (AT) at 6cm. Subsequently, a *Rosat* PSPC pointed X-ray observation was obtained for the cluster in 1993.

Send offprint requests to: H. Liang

In section 2, we present the *Rosat* PSPC data and the results of the analysis of both the flux densities of the discrete sources and the cluster X-ray surface brightness and temperature. In section 3, we calculate the total mass, gas mass and compare the X-ray and optical results. In section 4 we present the radio images at 1.4 and 4.9 GHz. In section 5, both limits on the radiation pressures due to the synchrotron emission and the X-ray thermal pressure are calculated. A value of $H_0 = 50 \text{ km s}^{-1} \text{ Mpc}^{-1}$ and $q_0 = 0.5$ are used throughout the paper.

2. X-ray Observations

A2717 was observed with the *Rosat* PSPC in June 1993 with a total integration time of 13.7 ksec. The PSPC has a field of view of 2° and is sensitive to photons with energy between 0.1 and 2.4 keV. The pointing centre was 00 03 19.2 -35 57 00 (J2000.0). The resolution of the PSPC is $\sim 20''$ at the centre of the detector at ~ 1.2 keV. The resolution degrades with decreasing energies and increasing distance from the detector centre.

2.1. Analysis of the X-ray data

The *Rosat* PSPC data was analysed using the EXSAS package (Zimmermann *et al.* 1994) in MIDAS. Discrete sources were detected first and subtracted from the data, so that they can be removed from the intracluster gas emission.

2.1.1. Discrete sources

The discrete sources were detected from a broad band image (including photons of energy from ~ 0.11 to ~ 2.35 keV) of $15''$ pixels excluding the regions affected by the support ribs of the detector. The sources were detected using a sliding window source detection technique whereby a 3×3 pixels window was slid over the image. The source counts were obtained from this sliding window and background counts were determined from the surrounding 16 pixels. This method is best suited for the detection of point or slightly extended sources. Finally a maximum likelihood method (Craddace *et al.* 1988) was applied to the sources detected to ascertain the reality and the extension of the sources. Table 3 lists all the sources found with maximum likelihood parameter > 10 . These sources were also scanned by eye and found to be consistent with real sources. None of the sources in Table 3 can be considered as extended. The positions and count rates for the sources are listed in Table 3. Correlations of the X-ray point sources with the SIMBAD and NED on-line catalogues were made, but no identification was found. A search through the *COSMOS* source list with an error radius of $20''$ produced a number of identifications. The optical position and magnitudes of the identified objects within the error radius are tabulated in Table 4.

In order to separate the contributions from the discrete sources and that of the cluster, we subtract the discrete sources found above, from the photon events file before making images of the field in a soft (0.1-0.4 keV) and a hard (0.4-2 keV) band (Figure 1). The peak of the hard image was identified with the central D-galaxy within uncertainty limits. The hard image peaks at 00 03 12.5 -35 56 02 which is $11''$ north of the optical position of the D-galaxy. The majority of the discrete sources

Table 3. Discrete X-ray sources in the field of A2717

source	α (2000.0)			δ (2000.0)			f_x counts/s
	h	m	s	°	'	''	
1	00	04	08.31	-35	54	48.7	0.00750
3	00	03	59.68	-35	56	48.4	0.00591
4	00	03	33.94	-36	07	34.2	0.01081
5	00	03	49.99	-36	07	45.5	0.00677
6	00	03	29.57	-36	11	46.3	0.00864
7	00	02	08.93	-35	41	58.0	0.01604
8	00	02	41.79	-35	55	27.9	0.00420
9	00	01	49.85	-35	57	00.7	0.01212
10	00	03	13.27	-36	01	46.3	0.00529
11	00	04	11.97	-36	02	26.6	0.00434
12	00	04	39.22	-36	02	37.6	0.00874
13	00	02	10.62	-36	04	20.6	0.00495
14	00	04	12.55	-36	06	09.5	0.00318
15	00	04	18.88	-36	10	38.9	0.00811
16	00	04	08.32	-35	32	19.2	0.01389
17	00	01	01.24	-35	46	38.8	0.03869
18	00	00	52.40	-35	58	33.7	0.01708
19	00	02	22.82	-36	29	18.5	0.02162
20	00	01	41.08	-36	03	04.3	0.01124
21	00	01	05.12	-36	17	52.1	0.01965

Explanation of columns: col.(1) gives the source sequence number; col.(2) & (3) gives the right ascension and declination of the X-ray source positions in J2000.0 coordinates; col.(4) gives the X-ray flux in count rates.

falling within the central $\sim 45''$ panel of the detector are systematically found to be between $5'' - 15''$ north of their optical counter part, suggesting a possible systematic error of $\sim 10''$ in the *Rosat* positions. A similar discrepancy of $11'' \times 16''$ between *Rosat* PSPC positions and optical positions was found by Pinkney *et al.* (1994). The peak of the soft image was displaced from that of the hard image and the D-galaxy, but coincides with a faint galaxy (see Figure 1). This displacement is consistent with the galaxy being an X-ray source with a spectrum considerably softer than the cluster (*e.g.* an AGN). This soft source was not detected with the above detection algorithm in the broad-band because of the soft source spectrum and the proximity of the source to the centre of the cluster emission which was predominately composed of hard photons. The position of the soft source was 00 03 16.2 -35 56 12 (J2000.0).

There were 2 Abell clusters, A4074 and S1170, and a galaxy group ESO 349-26 that were identified with X-ray sources near the edge of the detector. These sources were not detected using the formal detecting methods described above, owing to the proximity of the sources to the edge of the detector.

2.1.2. The Cluster

The *Rosat* PSPC has limited sensitivity in the high energy part of the X-ray spectra, namely > 2.4 keV, thus it can only constrain the temperature of relatively cold clusters with high precision.

The total cluster spectrum was obtained by including all the photons within a radius of $500''$ (*i.e.* 0.65 Mpc) but exclud-

Table 4. Optical I.D. of the discrete X-ray sources

source	α (2000.0)			δ (2000.0)			Δr "	B_j	class
	h	m	s	°	'	"			
1	00	04	08.34	-35	54	50.4	1.8	21.3	
	00	04	08.01	-35	54	41.4	8.2	21.9	
3	00	03	59.09	-35	57	05.1	18.2	22.0	
4	00	03	34.29	-36	07	44.8	11.4	18.7	s
5	00	03	50.65	-36	07	57.5	14.4	15.0	s
6	00	03	29.89	-36	11	46.9	4.0	21.1	g
	00	03	29.97	-36	12	03.6	17.4	19.6	s
7	00	02	09.28	-35	42	4.80	8.1	19.1	s
	00	02	08.11	-35	42	11.3	16.6	22.0	
8	00	02	41.63	-35	55	37.4	9.7	21.5	
	00	02	43.05	-35	55	37.7	18.2	22.5	
9	00	01	49.51	-35	57	16.7	16.5	18.0	s
10	00	03	13.39	-36	01	53.4	7.3	21.6	
	00	03	12.31	-36	01	35.1	16.2	17.5	s
11	00	04	12.20	-36	02	19.2	7.9	19.8	g
	00	04	11.79	-36	02	07.8	18.8	17.2	s
	00	04	12.20	-36	02	14.9	11.7	18.3	s
12	00	04	40.46	-36	02	43.0	16.0	18.6	s
13	00	02	10.60	-36	04	24.1	3.5	21.7	
15	00	04	18.59	-36	10	44.6	6.7	22.8	
17	00	01	01.66	-35	46	25.8	14.0	21.8	
18	00	00	50.99	-35	58	36.5	17.4	22.9	
20	00	01	41.24	-36	03	10.6	6.6	18.3	s
	00	01	42.29	-36	03	12.6	17.0	20.4	g
21	00	01	05.45	-36	17	52.9	4.1	11.6	s

Explanation of columns: Col.(1) gives the source sequence number; col.(2) & (3) gives the optical position of all the I.D.s found within the error radius of the X-ray position; col.(3) gives the distance in arcseconds between the X-ray position and the optical objects found with COSMOS; col.(4) gives the optical magnitude; col.(5) gives the classification of the objects given by COSMOS where it was able to make a clear distinction between a star ("s") and a galaxy ("g").

ing all the regions contaminated by the discrete sources, i.e. a circular area with a radius of the FWHM of the PSF at the position of the discrete source. The background spectrum was calculated from an annulus centred at the cluster centre and between a radius of 1750" and 2250".

The X-ray total flux and temperature were derived by fitting a Raymond-Smith spectrum with galactic absorption to the spectrum, using a program kindly provided by M. Arnaud. A χ^2 fit was made by allowing the X-ray emission measure, temperature and the neutral hydrogen column density to vary but fixing the abundance. A change in abundance between 0.3 to 0.5 only produced a 0.1 keV change in the best fit temperature. For an abundance of 0.3, the best fit found for the temperature is shown in Table 5 which is rather low for a cluster. The neutral hydrogen density was found to be $N_H = (1.56 \pm 0.13) \times 10^{20} \text{ cm}^2$ as compared to $N_H = 1.12 \times 10^{20} \text{ cm}^2$ from the radio surveys (Stark *et al.* 1992). The X-ray temperature was very well constrained and relatively independent of N_H .

The cluster surface brightness was obtained by first sub-

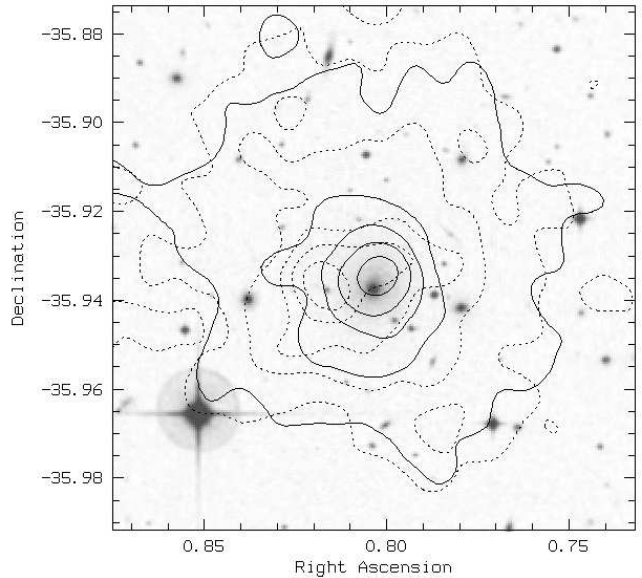


Fig. 1. The X-ray soft and hard contour images are superimposed on the digitised sky-survey (SERC J plates) image of the field. The axes are in decimal degrees. The X-ray maps have been smoothed with a Gaussian filter of FWHM $25'' \times 25''$. The hard-band image (0.4–2keV) is represented by solid contours of levels (1.2, 4.0, 6.8, 10.8) $\times 10^{-6} \text{ counts s}^{-1} \text{ arcsec}^{-2}$; the soft-band image (0.1–0.4keV) is represented by the dotted contours of levels (0.8, 1.6, 2.4, 3.2) $\times 10^{-6} \text{ counts s}^{-1} \text{ arcsec}^{-2}$; and the optical image is in grey-scales. The central D-galaxy is identified with the peak of the hard image, whereas the peak of the soft image is identified with a faint galaxy and is displaced from the peak of the hard image.

Table 5. Results from X-ray analysis of A2717

Centre (J2000.0)	RA = 00 03 12.5
	Dec = -35 56 02
T_g	$1.9_{-0.2}^{+0.3} \times 10^7 \text{ K}$
N_H	$(1.56 \pm 0.13) \times 10^{20} \text{ cm}^{-2}$
$n_{e,0}$	$9.6 \times 10^{-3} \text{ cm}^{-3}$
β	0.484
r_c	0.047 Mpc
$f_{x[0.1,2.4]keV}$ (0.65 Mpc)	$6.5 \times 10^{-12} \text{ erg s}^{-1} \text{ cm}^{-2}$
$L_{x[0.1,2.4]keV}$ (1.3 Mpc)	$7.8 \times 10^{43} \text{ erg s}^{-1}$
M_{gas} (1.3 Mpc)	$3.3 \times 10^{13} M_\odot$
M_{tot} (1.3 Mpc)	$1.1 \times 10^{14} M_\odot$
M_{tot}/L_B (1.3 Mpc)	77

tracting the point X-ray sources from the X-ray photon events file and producing a sky subtracted azimuthally averaged count rate profile (see Figure 2). Since the PSPC has a much lower background level in the hard band and the cluster emission tends to dominate the hard band, we have chosen only the data between channels 42 to 201 (~ 0.4 –2 keV) to produce the surface brightness profile.

The radially averaged X-ray surface brightness profile after the deconvolution of the PSF, was well fitted by a function of the form :

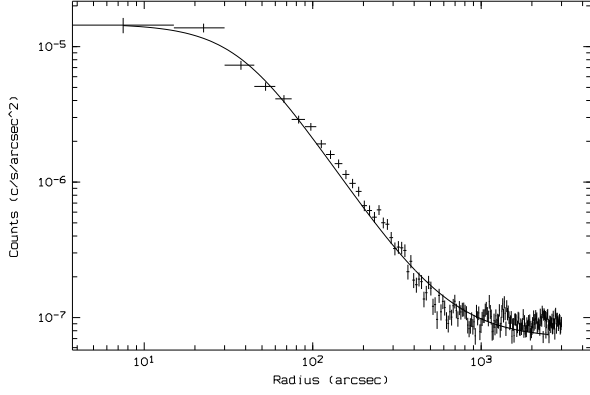


Fig. 2. The cluster X-ray surface brightness profile in the energy range of 0.4-2 keV. The data points with error bars are shown along with the cluster model X-ray surface brightness profile (including background) after convolution with the PSF (solid line).

$$S_x(r) = S_{x,0} [1 + (r/r_c)^2]^{-3\beta+1/2} \quad (1)$$

with $\beta = 0.484$ and core radius $r_c = 35.5''$ or 0.047 Mpc.

3. Mass distributions

In this section we will describe the method we used to deduce the cluster total mass, gas mass and other associated physical parameters from the X-ray data and compare some of these parameters (e.g. velocity dispersion) with the optical data available. We will assume that the gas is in hydrostatic equilibrium and isothermal. The X-ray surface brightness given in equation 1 corresponds exactly to a gas distribution of

$$\rho_g/\rho_{g,0} = [1 + (\frac{r}{r_c})^2]^{-3\beta/2} \quad (2)$$

if the gas extends all the way to infinity. Through the equation of hydrostatic equilibrium, the gas distribution is related to the cluster gravitational potential ϕ as follows:

$$\rho_g/\rho_{g,0} = \exp[\frac{\mu m_p}{k T_g} (\phi_0 - \phi)] \quad (3)$$

where T_g is the gas temperature, m_p is the proton mass and μ is the mean molecular weight of the gas in proton mass units. Thus the cluster gravitational potential corresponding to the gas distribution of equation 2 is given by

$$\phi(r) - \phi_0 = \frac{3\sigma_0^2}{2} \ln[1 + (\frac{r}{r_c})^2]. \quad (4)$$

where σ_0 is the central 3-D velocity dispersion and is related to β through $\beta = \frac{\mu m_p \sigma_0^2}{k T_g}$.

Thus from Poisson's equation the total mass density is given by:

$$\rho_{tot}(r) = \frac{3\beta k T_g}{4\pi \mu m_p G r_c^2} \frac{3 + (r/r_c)^2}{[1 + (r/r_c)^2]^2} \quad (5)$$

and the cluster total mass is given by:

$$M_{tot}(r) = \frac{3\beta k T_g r_c}{\mu m_p G} \frac{(r/r_c)^3}{1 + (r/r_c)^2} \quad (6)$$

From the X-ray spectral data, we found the best estimate emission measure and temperature assuming Raymond-Smith spectra. Thus we have the X-ray flux, f_x , within a radius of $500''$ (i.e. 0.65 Mpc) over the *Rosat* energy band of [0.1,2.4] keV, from the spectral data. The X-ray surface brightness profile given in Figure 2 gives the shape of the profile, namely β and r_c . The central electron density $n_{e,0}$ can then be estimated from f_x , β and r_c (see Table 5). The cluster total mass and gas mass within the radius of $1000''$ (or 1.3 Mpc), i.e. the maximum extent where there is still detectable X-ray emission from the surface brightness profile, are given in Table 5. The radius of $1000''$ (or 1.3 Mpc) is chosen such that no extrapolation would be necessary in calculating the masses from the X-ray data. The total X-ray luminosity calculated up to the same radius of 1.3 Mpc was found to be consistent with the $L_x - T_g$ relation given by Ebeling (1993).

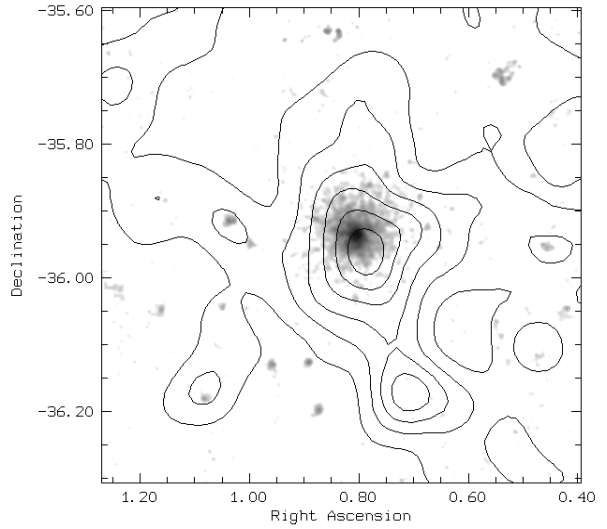


Fig. 3. An image of the *Rosat* PSPC image superimposed on the galaxy number counts isocontours (obtained from Colless 1987). The axes are in decimal degrees. The contour levels are (0.06, 0.12, 0.18, 0.24, 0.3, 0.36) galaxies arcmin⁻².

We compare the X-ray deduced velocity dispersion of the cluster with the measured galaxy velocity dispersion. From Jean's equation for a spherical, steady state system with isotropic velocity distribution, we can deduce the 3-D velocity dispersion σ from the potential given in equation 4 and the total mass density (equation 5) if the galaxy number distribution follows that of the total mass. Thus the 3-D velocity dispersion in this case is given by

$$\sigma^2(y) = \frac{1 + y^2/2}{1 + y^2/3} \sigma_0^2 \quad (7)$$

where $y = r/r_c$ is the 3-D radius in core radius units and σ_0 is the 3-D velocity dispersion at the centre. In producing the above analytic expression, we have assumed that the cluster

extends to infinity and that the galaxies can be treated as test particles in the cluster potential with a distribution that follows the mass. Figure 3 shows the galaxy number count isocontours overlaid on the X-ray image. The southern structure in the isopleth map was identified with a background group (Colless 1987). Note also the coincidence between the X-ray emission and the optical structures. Since the cluster is fairly regular, it can be circularly averaged to produce a galaxy number density distribution. We found that the galaxy density distribution thus deduced agreed well with the shape of the projected mass distribution, thus justifying the mass-follows-light assumption. The line of sight velocity dispersion σ_{los} , can be projected from the 3-D dispersion through (Merritt 1987):

$$\Sigma(x)\sigma_{los}^2(x) = 2 \int_x^\infty \rho_{tot}\sigma^2(y) \frac{ydy}{\sqrt{y^2 - x^2}} \quad (8)$$

where Σ is the projected mass density, $x = R/r_c$ is the projected radius in core radius units. Therefore, the line of sight velocity dispersion σ_{los} is given by

$$\sigma_{los}^2(x) = \frac{9}{8} \left[\frac{1 + 2x^2/3}{1 + x^2/2} \right] \sigma_0^2 \quad (9)$$

(see Appendix of Mellier *et al* 1994, but note there is a misprint). However, the measured velocity dispersion in most cases is the average of σ_{los} within a certain radius. We derive the $\overline{\sigma_{los}}$ from the above and obtain

$$\overline{\sigma_{los}^2}(< x) = \frac{3}{4} \left(2 + \frac{1}{x^2} \right) \sigma_0^2 \quad (10)$$

We can thus estimate σ_0^2 from β and T_g and deduce $\overline{\sigma_{los}}(< 2 \text{ Mpc}) = 429 \pm_{-22}^{+32} \text{ km s}^{-1}$. Note that $\overline{\sigma_{los}^2}(< 2 \text{ Mpc}) = 1.5\sigma_0^2$, thus the difference is significant and the usual assumption of a constant velocity dispersion with radius could easily produce the difference between β_{spec} and β_{imag} noted in many clusters (Sarazin 1988). However, in the case of A2717, this difference is still not large enough to obtain consistency. The measured $\overline{\sigma_{los}}$ of A2717 from the galaxies within a radius of 2 Mpc was $\overline{\sigma_{los}} = 547_{-72}^{+92} \text{ km s}^{-1}$ (Colless *et al.* 1987). Thus the measured galaxy velocity dispersion was slightly higher than that deduced from the X-ray data. As mentioned in Colless *et al.* (1987), there is evidence of foreground and background groups that may have contaminated the measurements and thus overestimate the velocity dispersion.

Given the electron density and gas temperature we can calculate the central cooling time, t_{cool} , given by

$$t_{cool} \sim 8.5 \times 10^{10} \left(\frac{n_e}{10^{-3} \text{ cm}^{-3}} \right)^{-1} \left(\frac{T_g}{10^8 \text{ K}} \right)^{0.5} \text{ yr} \quad (11)$$

(Sarazin 1988) and for A2717, it amounts to ~ 3.4 Gyr which is smaller than the Hubble time (~ 10 Gyr). Thus in the absence of heating, cooling occurs within the centre of the cluster with a cooling radius of ~ 90 kpc. Pending further evidence of the existence of a cooling flow, this maybe one of the few cases where a WAT is found in a cooling flow cluster (c.f. Burns 1990).

4. Radio Observations

The WAT identified with the central D-galaxy was observed at the Molonglo Observatory Synthesis Telescope (MOST) at 843

MHz with a resolution of $43'' \times 73''$ in 1988, at the VLA at 1.4 GHz in the B/C configuration (resolution of $9'' \times 10''$) and at 4.9 GHz in the C/D configuration (resolution of $9'' \times 10''$) in 1989. The central parts of the source was also imaged at the Australia Telescope at a high resolution ($2'' \times 4''$) with a 6km array in 1992. In this paper, we will concentrate on the VLA images.

4.1. Analysis of Radio Data

The 1.4 GHz image was calibrated using 3C48 as the primary calibrator, but a different primary calibrator 3C286 was used for the 4.9 GHz observation. The images were processed using the standard AIPS package for radio synthesis data. Figure 4 shows the 1.4 GHz image superimposed on the X-ray image. The two tails are reasonably symmetrically located around the centre of the cluster and are bending southwards. The 4.9 GHz image smoothed to the same resolution as the 1.4 GHz image is shown in Figure 5. The eastern tail disappears below the sensitivity limit in this image, due to the steepness of the spectral index in the tail. The spectral index steepens dramatically from the flat core ($\alpha \sim -0.5$) to the lobes where $\alpha \sim -3$. The linear size of the WAT was estimated from the 1.4 GHz image to be > 360 kpc. The total radio luminosity of the WAT at 1.4 GHz is estimated to be $5.8 \times 10^{24} \text{ W Hz}^{-1}$, which is just below the FR break. Such moderate radio powers are typical of radio sources associated with cluster dominant galaxies (Heckman 1980) and of medium sized WATs (Burns 1986).

A comparison of the redshifts of the D-galaxy and the cluster shows that the D-galaxy is moving away from us at a speed of $\sim 300 \text{ km s}^{-1}$. In general the galaxies with which the WATs are associated move through the intracluster medium (ICM) very slowly, if at all, rarely obtaining velocities greater than about a half their stellar dispersion (which corresponds to $\approx 200 \text{ km s}^{-1}$) with respect to the cluster centre (Burns 1982, Eilek 1984, Bothun 1990). WATs were thought to be bent by the ICM through their slow motion in the medium. However, recent detailed studies by O'Donoghue *et al.* (1993) have shown that this standard model breaks down when examined in detail using the current theories of the physics of the jets. Alternative models suggest that tails may be bent by the bulk flow of velocities $\sim 1000 \text{ km s}^{-1}$ in the ICM due to subcluster mergings (Burns *et al.* 1986; O'Donoghue *et al.* 1993; Roettiger *et al.* 1993).

5. Pressure balance

5.1. Thermal pressure

The thermal pressure due to the intracluster medium can be calculated from the PSPC X-ray data by assuming that the gas is isothermal and that the ion and electron temperatures are the same. Thus the thermal pressure is approximated by $P_{th} \sim 2n_e k T_g$, where T_g and n_e are estimated from the X-ray surface brightness profile and the X-ray spectra in section 2. Figure 6 shows the thermal pressure as a function of radius.

5.2. Minimum radiation pressure

The radio data enable the minimum internal pressure of the tails to be calculated (Burbidge 1958). The tails would be at a minimum pressure when the equipartition condition is satisfied, namely the energy density of the relativistic particles is

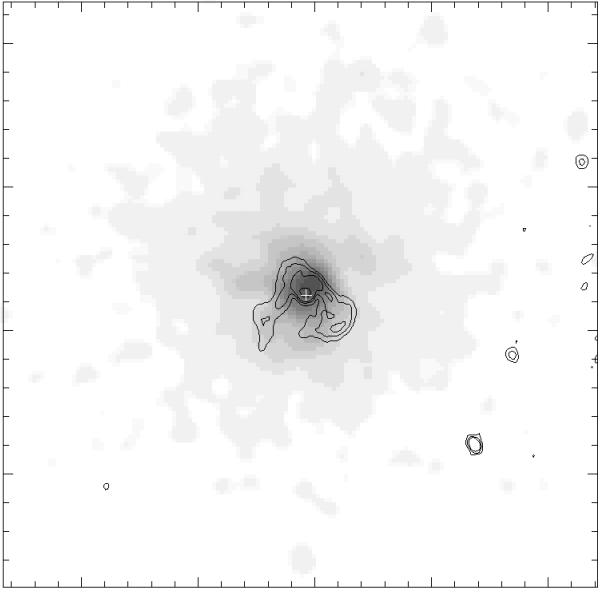


Fig. 4. Radio VLA image of the WAT at 1.4 GHz superimposed on the *Rosat* PSPC X-ray image in the hard band. The field size is $12' \times 12'$ with east to the left and north upwards. The radio images is in contours of (0.8, 3.0, 7.0, 50.0) mJy beam^{-1} . The radio image was smoothed by a Gaussian to a resolution of $\text{FWHM } 11'' \times 11''$ (c.f. Fig. 5).

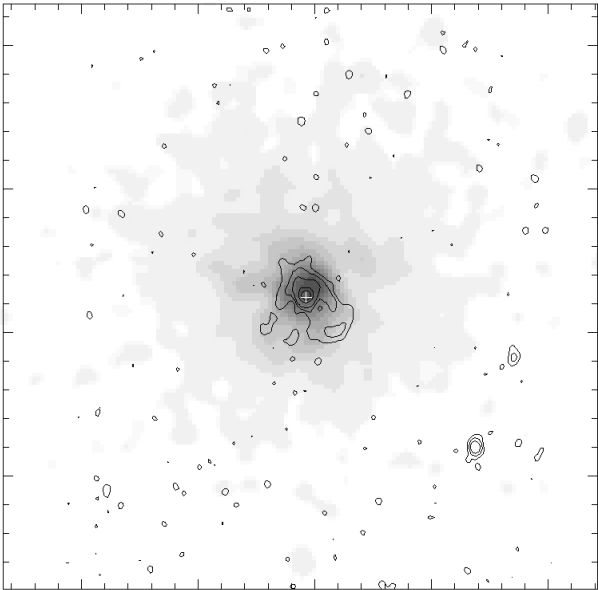


Fig. 5. A VLA contour image of the WAT at 4.9 GHz superimposed on a grey scale hard band PSPC image. The field size is $12' \times 12'$ with east to the left and north upwards. The radio contours are (0.07, 0.3, 0.8, 1.0, 2.0) mJy beam^{-1} . The radio image was smoothed by a Gaussian to a resolution of $\text{FWHM } 11'' \times 11''$ (c.f. Fig. 4).

equal to that of the magnetic field (Pacholczyk 1970). Indeed given the thermal pressure of the surrounding medium, we can verify if the tails are in equipartition. We have adopted the method given by Killeen *et al.* (1988) for calculating the minimum pressure. The following assumption were made: 1) the jets are perpendicular to the line of sight and the magnetic field lines are perpendicular to the line of sight; 2) the energy ratio k between relativistic electrons and relativistic protons plus thermal particles is 1; 3) the source spectra is a power law extending from 10 MHz to 100 GHz with a spectral index of $\alpha = -2.3$; 4) the filling factor is 1. Amongst the above assumptions, the two most uncertain factors are k and the filling factor. The parameter k can range from 1 to 2000 (Pacholczyk 1970) and a factor of 100 in k produces roughly an order of magnitude difference in P_{min} . The filling factor can easily be < 1 . However, an increase in k increases P_{min} and a decrease in the filling factor increases P_{min} . Thus by choosing $k = 1$ and filling factor = 1, we have really calculated the minimum P_{min} .

S

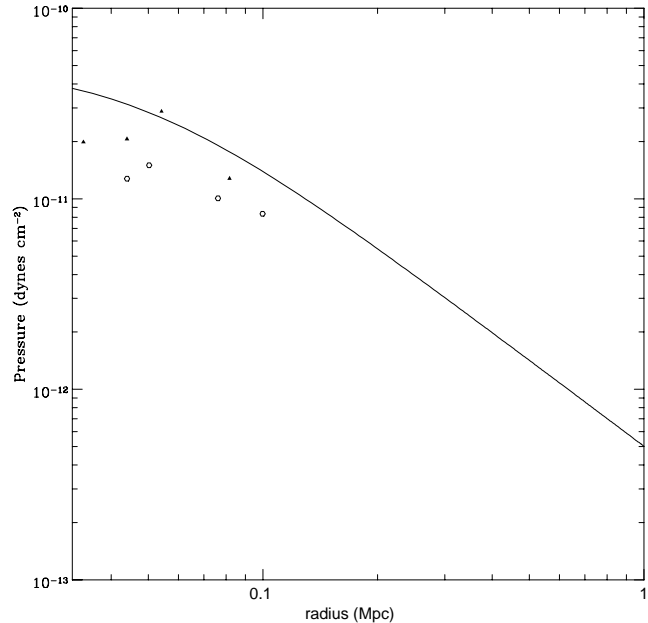


Fig. 6. A comparison of the thermal X-ray pressure (solid curve) with that of the minimum radiation pressure. The filled triangles show the minimum pressure for each slice of the western jet and the open circles are for that of the eastern jet.

In order to calculate the internal pressure exerted by the particles in the radio source, the 1.4 GHz image was smoothed with a circular beam of $11'' \times 11''$ and Gaussians were fit to slices perpendicular to the jet to estimate the peak flux density and size of each slice. The minimum radiation pressure was calculated for each slice using a program kindly supplied by Geoff Bicknell (see Figure 6). An average spectral index of $\alpha \sim -2.3$ was used for each slice of the tails. Given the uncertainties involved, Figure 6 shows that the minimum pressure deduced from the radio data is in good agreement with the X-ray pressure, i.e. within a factor of 2-3. This suggests that the tails are likely to be in equipartition, if we assume that the tails are in pressure equilibrium with the X-ray gas. Note that

the minimum pressure plotted are truly the lower limits, due to the choice of k and filling factor. Feretti *et al.* (1992) showed in a study of ~ 40 tailed radio sources, including WATs and NATs, that the thermal pressure is always either comparable to or higher than the minimum P_{min} . A study of 22 low radio luminosity sources by Morganti *et al.* (1988) had found a similar result, suggesting that low luminosity radio sources can be confined by thermal pressure alone.

6. Conclusions

We have presented the X-ray, radio data of the cluster A2717 and analysed the data along with the optical data available in the literature. The cluster has a total X-ray luminosity of 7.8×10^{43} ergs $^{-1}$ within a radius of 1.3 Mpc and a well determined temperature of $1.9^{+0.3}_{-0.2} \times 10^7$ K. The X-ray determined total mass was $\sim 1.1 \times 10^{14} M_{\odot}$ within 1.3 Mpc, comparable to the virial mass given all the uncertainties. The gas mass was found to be $\sim 30\%$ of the total mass.

The thermal pressure from the ICM was found to be comparable to the minimum pressure in the tails of the radio galaxy associated with the central D galaxy, suggesting that the WAT is most likely to be in equipartition with the surrounding media. The X-ray image of the cluster gas at the PSPC resolution was almost structureless and no obvious interaction between the WAT and the ICM was seen. To obtain detailed morphological information that would show the possible interaction between the radio galaxy and the X-ray medium, as seen in the case of NGC 1275 (Böhringer *et al.* 1993), we need a higher resolution X-ray image.

Acknowledgements: We would like to thank Monique Arnaud for kindly providing the X-ray spectral analysis program, Geoff Bicknell and Neil Killeen for their program to calculate the minimum pressure and Matthew Colless for useful discussions on the optical data. We acknowledge the use of the COSMOS/UKST Southern Sky Catalogue supplied by the Anglo-Australian Observatory. HL acknowledges the support of the Australia-France collaboration fund.

References

- Abell G.O., Corwin H.G., Olowin O.P., 1989, ApJS 70, 1
 Allen S.W., Edge A.C., Fabian A.C., Böhringer H., Crawford C.S., Ebeling H., Johnstone R.M., Taylor T., Schwarz R.A., 1992, MNRAS 259, 67
 Biviano A., Girardi M., Giuricin G., Mardirossian F., Mezzetti M., 1992, ApJ 396, 35
 Böhringer H., Voges W., Fabian A.C., Edge A.C., Neumann D.M., 1993, MNRAS 264, L25
 Bothun G.D., Schombert J.M., 1990, ApJ 360, 436
 Burbidge G.R., 1958, ApJ 129, 841
 Burns J.O., Eilek J.A., Owen F.N., 1982, in *Extragalactic Radio Sources*, eds. D.S. Heeschen and C.M. Wade, 45
 Burns J.O., O’Dea C.P., Gregory S.A., Balonek T.J., 1986, ApJ, 307, 73.
 Burns J.O., 1990, AJ 99, 14
 Colless M.M., *A Dynamical Study of Rich Clusters*, 1987, Ph.D. Thesis, University of Cambridge
 Colless M., Hewett P., 1987, MNRAS 224, 453
 Colless M., 1989, MNRAS 237, 799
 Cruddace R.G., Hasinger G.R. and Schmitt J.H., 1988, in *Astronomy from Large Databases*, ed. Murtagh F. and Heck A., 177
 Ebeling H., 1993, Ph.D. Thesis, Ludwig Maximilians Universität Munich
 Eilek J.A., Burns J.O., O’Dea C.P., Owen F.N., 1984, ApJ 278, 37
 Fanaroff B.L., Riley J.M., 1974, MNRAS 167, 31
 Feretti L., Perola G., Fanti R., 1992, A&A 265, 9
 Girardi M., Biviano A., Giuricin G., Mardirossian F., Mezzetti M., 1993, ApJ 404,38
 Heckman T.M., 1980, A&A 87, 142
 Killeen N.E.B., Bicknell G.V., Ekers R.D., 1988, ApJ 325, 180
 Mellier Y., Fort B., Kneib J., 1993, ApJ 407, 33
 Merritt D., 1987, ApJ 313, 121
 Morganti R., Fanti R., Gioia I.M., Harris D.E., Parma P., de Ruiter H., 1988, A&A 189, 11.
 Norman M., Burns J., Sulkanen M., 1988, Nature 335, 146
 O’Donoghue A., Eilek J., Owen F., 1990, ApJS 72, 750
 O’Donoghue A., Eilek J., Owen F., 1993, ApJ 408, 428
 Owen F.N., White R.A., Hildrup K.C., Hanisch R.J., 1982, AJ 87, 1083
 Pacholczyk A.G., 1970, *Radio Astrophysics* (San Francisco: Freeman)
 Pedlar A., Ghataure H.S., Davies R.D., Harrison B.A.N., Perley R., Crane P.C., Unger S.W., 1990, MNRAS 246, 477.
 Pinkney J., Burns J.O., Hill J.M., 1994, AJ 108, 2031
 Roettiger K., Burns J.O., Loken C., 1993, ApJ 407, L53.
 Sarazin C.L., 1988, in *X-ray Emission from Clusters of Galaxies*, Cambridge University Press
 Stark A.A., Gammie C.F., Wilson R.W., Bailey J., Linke R.A., Heiles C., Hurwitz M., 1992, ApJS 79, 77
 Zhao J.H., Burns J.O., Owen F.N., 1989, AJ 98, 64
 Zimmermann H.U., Becker W., Belloni T., Döbereiner S., Izzo C., Kahabka P., Schwenker O., 1994, MPE Report No. 257, available through: <http://www.rosat.mpe-garching.mpg.de/doe/exsas.html>